Peak loads during dynamic ice-structure interaction caused by rapid ice strengthening at near-zero relative velocity

Owen, Cody C.; Hammer, Tim C.; Hendrikse, Hayo

DOI
10.1016/j.coldregions.2023.103864

Publication date
2023

Document Version
Final published version

Published in
Cold Regions Science and Technology

Cold Regions Science and Technology 211 (2023) 103864

Contents lists available at ScienceDirect

Cold Regions Science and Technology

journal homepage: www.elsevier.com/locate/coldregions

Peak loads during dynamic ice-structure interaction caused by rapid ice strengthening at near-zero relative velocity

Cody C. Owen *, Tim C. Hammer, Hayo Hendrikse

Department of Hydraulic Engineering, Delft University of Technology, Delft, the Netherlands

ARTICLE INFO

Keywords:
Ice-induced vibration
Ice crushing
Model tests
Compliance effect
Velocity effect

ABSTRACT

A series of ice penetration tests with a rigid structure, with controlled oscillation, and with a single-degree-of-freedom structure were performed to investigate the peak load-velocity dependence for ethanol-doped model ice during a test campaign at the Aalto Ice and Wave Tank. For the rigid structure and controlled-oscillation tests, the ice drift speed ranged between 1 and 150 mm s^{-1}. In the controlled-oscillation tests, amplitudes of oscillation between 0.40 and 15.90 mm and frequencies of oscillation between 0.143 and 4 Hz were prescribed such that the relative velocity between ice and structure never became negative. A constant ice drift deceleration experiment with a single-degree-of-freedom structure was performed to investigate the development of frequency lock-in and intermittent crushing in the model ice and compare the results with the rigid structure and controlled-oscillation tests. It was found that the peak load-velocity dependence identified in the rigid structure tests was not always uniquely defined as identified in the controlled-oscillation tests because the loading history affected the peak load at ice failure. A rapid strengthening of the ice developed at low relative velocity and carried over to high relative velocity until the ice failure dissipated the strengthening effect. The strengthening effect, observed in the rigid structure and controlled-oscillation tests, was also observed during frequency lock-in and intermittent crushing in the single-degree-of-freedom structure test. The observations in the present study indicate that the so-called velocity and compliance effects in ice-structure interaction originate from the same strengthening effect. It then follows that peak loads on compliant structures cannot exceed peak loads on rigid structures in the same ice conditions, with the only difference being that the peak loads on compliant structures occur at apparently higher far-field ice drift speeds due to the change in relative velocity.

1. Introduction

The magnitude of ice loads during indentation is known to be dependent on the relative velocity between ice and structure, or rate of loading, of the ice. This 'velocity effect' has been observed in experimental campaigns (Izumiyama et al., 1994; Kamesaki et al., 1996; Kärnä et al., 2008; Määttanen, 1981; Singh et al., 1990; Sodhi, 2001; Tsuchiya et al., 1985) and in full-scale as first shown by Peyton (1968) and later summarized by Jefferies et al. (2008) for multiple offshore structures. It has also been proposed that there exists a 'compliance effect,' related to the observation that loads during intermittent crushing on a flexible structure are typically higher than the loads on a rigid structure for the same far-field velocity (Kamesaki et al., 1996; Kärnä et al., 2008). A typical peak load-velocity curve as presented in Singh et al. (1990) is shown in Fig. 1, demonstrating both the velocity effect and the compliance effect.

The negative slope in the peak load-velocity dependence is often interpreted as a source of 'negative damping' and related to the development of ice-induced vibrations of compliant structures. Models for prediction of ice-induced vibrations sometimes assume a one-to-one (bijective) relation between peak load and velocity (Hetmanczyk et al., 2011; Kärnä, 1992; Määttänen, 1998; Withalm and Hoffmann, 2010). The definition of this relation is somewhat challenging though, given that the compliance effect requires the curve to be shifted with velocity for changes in mass, natural frequency, and damping of the structure. In modeling this is, for example, accounted for by shifting the position of the negative gradient along the velocity axis based on natural frequency of the structure (Huang and Liu, 2009). Ultimately, the question remains whether the peak load-relative-velocity relation in ice-structure interaction has a linear dependence on the stress-strain-rate

* Corresponding author at: Delft University of Technology, Faculty of Civil Engineering and Geosciences, Department of Hydraulic Engineering, Section of Offshore Engineering, Stevinweg 1, Delft 2628CN, the Netherlands.
E-mail address: c.c.owen@tudelft.nl (C.C. Owen).

https://doi.org/10.1016/j.coldregions.2023.103864
Received 24 January 2023; Received in revised form 13 March 2023; Accepted 11 April 2023
Available online 11 April 2023

relation as observed in uniaxial compression of ice.

Even when accounting for the compliance effect in defining the peak load-velocity dependence, there is a question if a bijective relation between peak loads and velocity is correct. Controlled-oscillation experiments (Hendrikse and Metrikine, 2016) showed indications that the loading history affects peak loads, though challenges with control and the absence of rigid penetration experiments did not allow firm conclusions to be drawn. Another question of relevance is if peak loads on a compliant structure can exceed those at the lowest speeds on rigid structures, or if the compliance effect is merely a different manifestation of the same effect responsible for the velocity effect as seen for rigid structures.

In the present study, results are introduced from ice penetration tests with a rigid structure and with controlled oscillation which were performed with the aim to answer two questions. First, does a load-history dependence exist for the peak load-velocity relation during ice penetration? Second, do the velocity effect and compliance effect originate from the same effect? Experiments with a single-degree-of-freedom (SDOF) structure were also conducted to investigate ice-induced vibrations in the same model ice as the rigid and controlled-oscillation tests. The results from the penetration experiments performed with the rigid structure, controlled oscillation, and SDOF structure in the present study show that peak loads depend on the amount of time spent at low relative velocities where a strengthening of the ice can develop. The term ice strengthening is herein defined as the consistent increase in mean and peak global ice-induced loads due to loading history.

The present study is structured as follows. Section 2 introduces the test campaign with a focus on the hybrid test setup used, the model ice properties, and the different types of tests conducted. Section 3 establishes the peak load-velocity dependence for the model ice based on rigid structure ice penetration tests. Section 4 establishes the peak load-velocity dependence from controlled-oscillation experiments and investigates the load-history effect. Section 5 shows the results from constant deceleration tests with a SDOF structure where the load-history effect appears during frequency lock-in (FLI) and intermittent crushing (ICR). The discussion, in Section 6, focusses on the effect of compliance on the load-velocity dependence, an explanation for the strengthening effect from the literature, and the representativeness of model ice as a substitute for naturally occurring or full-scale sea ice.

2. Test campaign description

The experiments analyzed in the present study were part of a large test campaign in the SHIVER project conducted at the Aalto Ice and Wave Tank. The tank is a 40 m by 40 m indoor facility where experiments with floating freshwater and ethanol-doped ice can be conducted. In the SHIVER campaign, which included the tests analyzed herein, ethanol-doped ice was used. Hendrikse et al. (2022b) give a detailed description of the experimental design, and materials and methods. The following sections summarize the most relevant information for the analysis in the present study.

2.1. Test setup

The real-time hybrid test setup combined mechanical and numerical components to allow for tests with a rigid structure, controlled-oscillation tests, and simulation of structural models in real-time (e.g. (Hammer et al., 2023, Hammer et al., 2022, Hammer et al., 2021; Hendrikse et al., 2022b, Hendrikse et al., 2022a; van den Berg et al., 2022)). Fig. 2 shows a photograph of the setup during testing and gives a schematic overview of the setup components. A rigid, cylindrical aluminum pile with a diameter of 200 mm penetrated the ice sheet. Ice-induced loads were identified from pile strains, which were measured with strain gauges located above the ice action point. The structural displacement at the ice action point was applied to the pile by bi-directional linear actuators. The pile displacements matched either the prescribed displacements of controlled oscillation or the calculated displacements of a simulated structure at the ice action point. In the case of a SDOF structure test, the response of the simulated structure to the measured ice-induced loads was numerically simulated on a microcontroller. The pile displacements were measured by displacement sensors. In the tests described in the present study, only pile displacement in the ice drift direction was modeled (y-direction as indicated in Fig. 2; cross-drift or x-direction was immobilized).

The real-time hybrid test setup was mounted to a carriage. The carriage was mounted to a bridge spanning the ice tank. The bridge was

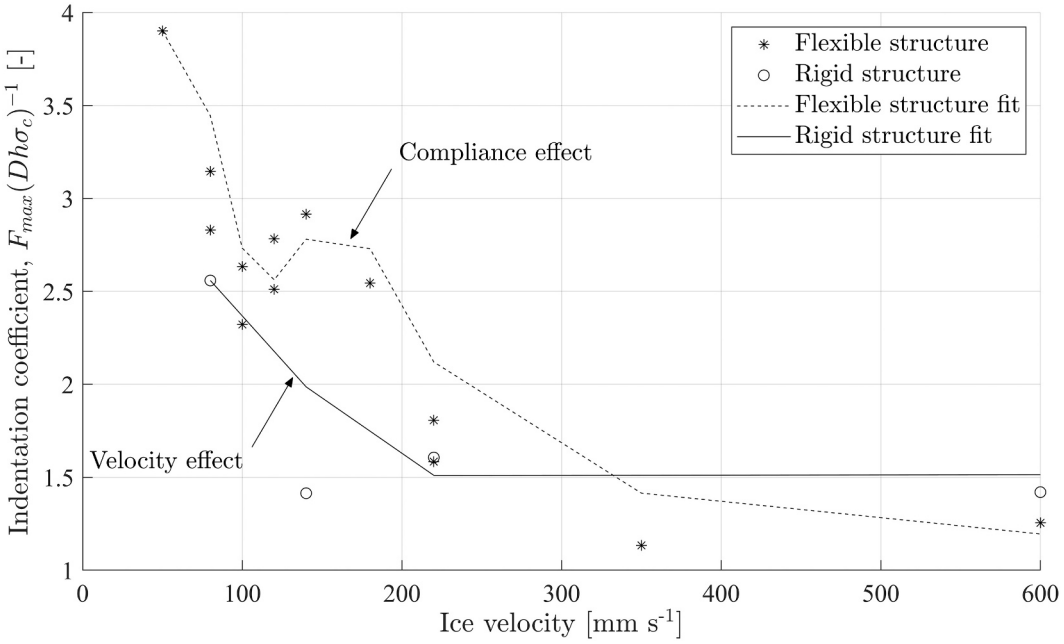

Fig. 1. Data replotted from Singh et al. (1990) showing the 'velocity effect' and 'compliance effect.' The indentation coefficient is defined as maximum excitation force F_{max} divided by width D, thickness h, and (uniaxial) compressive strength σ_c. The fitting is performed by applying a moving average, with window of two data points, using the mean indentation coefficient at each ice velocity.

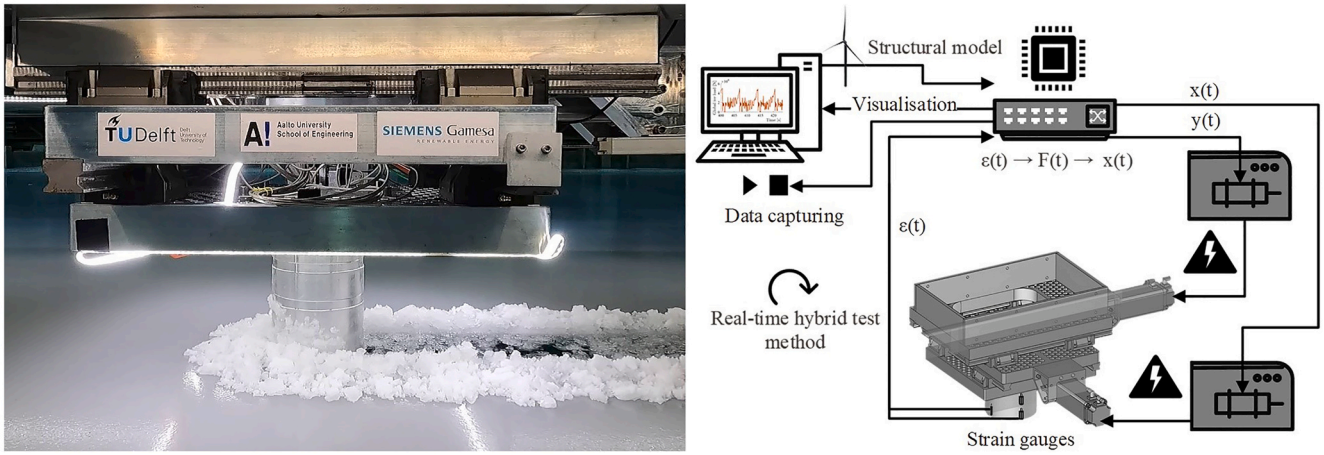

Fig. 2. Left: Photograph of the real-time hybrid test setup during testing, showing the cylindrical pile interacting with the ice. Right: Schematic overview of the real-time hybrid test setup (Hammer et al., 2021).

stationary for each test. Ice drift was achieved either 1) by moving the carriage along the bridge with prescribed speeds (5 mm s^{-1} to 150 mm s^{-1}); or 2) by the actuator, with the carriage stationary, for low speeds on the order of 1 mm s^{-1} for the rigid structure tests (1 mm s^{-1} to 10 mm s^{-1}, see Table A.2, Table A.3, and Table A.4). The resulting apparent ice drift was then opposite to the carriage movement direction or the actuator movement direction when the carriage was stationary. In the present study, movement of the carriage, or the actuator movement when the carriage was stationary for the rigid structure tests, is referred to as ice drift. The real-time hybrid test setup is referred to as the structure. The measured pile displacements relative to the carriage supporting the real-time hybrid test setup are termed the structural displacements.

During the tests, the global ice-induced loads and structural responses were measured with load cells, strain gauges, accelerometers, and displacement sensors. The analyses introduced in the present study use the externally-unfiltered global ice loads as identified by the strain gauges. The reader is referred to Hendrikse et al. (2022b) for more information about the real-time hybrid test setup.

2.2. Model ice

The model ice was created by spraying a fine mist of a water-ethanol mixture on a thin layer of initial ice, according to the following procedure: 1) Lower the tank temperature to −10 °C. 2) Remove the ice that has formed on the basin surface. 3) Refreeze the water surface for 20 min, forming a smooth, thin layer of ice. 4) Spray mist at −10 °C for 180 min, forming a layer of sprayed ice of 20 mm. 5) Harden the ice at −11 °C for a total of 150 freezing-degree-hours. The spraying water and the water in the ice tank had an ethanol content of 0.3%. The spraying process resulted in a fine grain structure that captured the ethanol in small pockets. The mean ice thickness in which the tests were performed was 30 mm.

The ice material properties were measured according to the International Towing Tank Conference recommended procedures and guidelines (ITTC, 2014). The flexural (σ_f) and compressive (σ_c) strengths of the ice were measured at the end of each test day. The effective elastic-strain modulus (E) was only measured on the 17th of June 2021 (only one of the two test days analyzed in this study). Table 1 shows the measured material properties. The effective elastic-strain modulus determination is dependent on the measured ice thickness, causing uncertainty in the measured value. The values between parentheses in Table 1 show the effective elastic-strain modulus variation following from an ice thickness change of ±5 mm. Refer to Hendrikse et al. (2022b) for more details on the material property measurements. It is noted that the ice material properties are mentioned here only for relative comparison with previous test campaigns, the values may not reflect the properties during actual testing at different moments during the day. Results from the rigid structure tests and results of continuous crushing from the SDOF structure tests give a good indication of ice strength during testing and, in the view of the authors, provide more relevant information for penetration experiments than the material properties in Table 1.

Table 1
Material properties of the ice on two of the three test days considered in the present study. The material properties were measured at the end of the test day.

Ice sheet date	σ_f [kPa]	σ_c [kPa]	E modulus [GPa]
17-6-2021	521	563	13 (7.8–24)
23-6-2021	444	658	–

2.3. Tests included in the analysis

The present study considers results from three types of tests (see Fig. 3). The first type concerns a rigid structure aimed at characterizing the velocity effect in ice loads, with ice drift speeds ranging from 1 mm s^{-1} to 150 mm s^{-1}. Table A.2 gives an overview of the tests with a rigid structure considered in the present study. The test IDs represent test identifiers which can be used to obtain the raw test data from the public dataset (Hendrikse et al., 2022b). The run name contains the test date and the run number. A run is a full passing of the carriage from one side of the ice tank to the other side. The runs are numbered consecutively starting from 1 on each test day. All tests with a rigid structure performed on the 17th and 23rd of June are analyzed in the present study.

The test data from rigid tests are used as a basis for comparison with the data from the controlled-oscillation tests. The controlled-oscillation tests employed a prescribed oscillation pattern of the structure resulting in the following structural displacement:

$$u_c(t) = A\sin(\omega_c t) \tag{1}$$

with $\omega_c = 2\pi f_c$ where u_c is the controlled displacement of the structure, A is a prescribed amplitude of oscillation (0.40 mm to 15.90 mm), and f_c is a prescribed frequency of oscillation (0.143 Hz to 4 Hz, see Table A.3). For the test, the amplitude and frequency were chosen such that the minimum relative velocity between ice and structure reached zero during a cycle of oscillation:

$$\frac{v_{ice}}{A\omega_c} = 1 \tag{2}$$

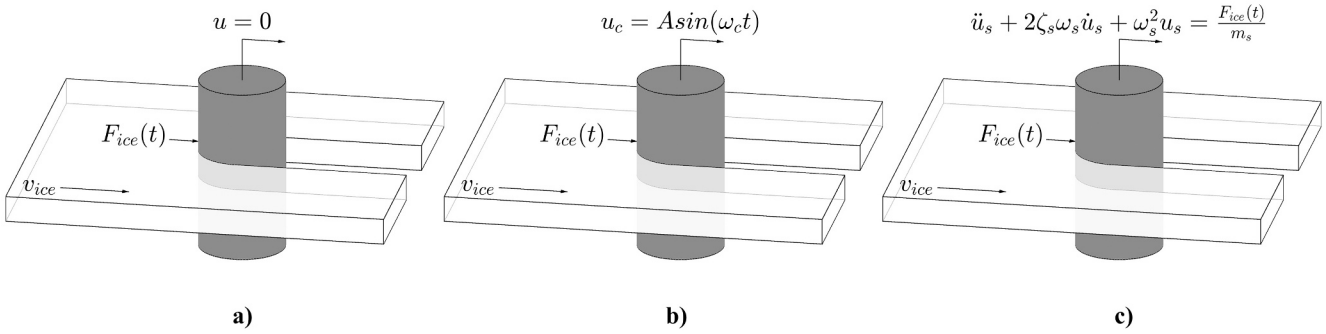

Fig. 3. Illustration of the three types of tests included in the analysis: a): rigid structure; b): controlled-oscillation; c): single-degree-of-freedom structure. Denoted in the illustrations are the far-field ice drift speed v_{ice}, ice load at the ice action point $F_{ice}(t)$, the structural response u, controlled-oscillation amplitude A and frequency ω_c, and single-degree-of-freedom structural properties of damping as fraction of critical ζ_s, natural frequency ω_s, and mass m_s.

where v_{ice} is the ice drift speed (constant carriage speed during the controlled-oscillation tests). The controlled-oscillation tests were performed in the same ice sheet as the rigid structure tests, often in the same run. An overview of the controlled-oscillation tests is shown in Table A.3. The test matrix was derived with frequencies of oscillation resembling those of modes of an offshore wind turbine, and by repeating experiments previously conducted in another ice tank (Hendrikse and Metrikine, 2016).

Lastly, results from a constant deceleration test with a SDOF structure are included to investigate the compliance effect for comparison with the observations from the rigid structure and controlled-oscillation tests. Multiple tests have been performed and analyzed by van den Berg et al. (2022). Herein, only a single example is included (see Table A.4).

3. The load-velocity dependence from rigid structure tests

The load-velocity dependence from the rigid structure indentation tests on the 17th and 23rd of June are shown in Fig. 4 and Fig. 5, respectively. The velocity effect is found in the peak loads at low velocities (< 3 mm s^{-1}) being higher than those at high velocities (> 3 mm s^{-1}) by about 50%. For the mean loads, the effect is almost 100%. The higher loads at low rates are mainly due to a higher mean load. This becomes clear when the results per velocity are plotted with the mean load subtracted (see Fig. 4b and Fig. 5b). The peak load range as a scatter from the mean seems to be rather independent of velocity on both days. It is interesting to note that, despite the similar ice growth procedure of the model ice, the mean loads on the 17th of June were 50% higher than those on the 23rd of June. The main cause for the disparity in means loads was the difference in freezing-degree-hours at the moment of the testing during the day. The majority of the testing on the 17th of June occurred about six hours later in the day than on the 23rd of June (see Table A.2). However, the exact air and ice temperature profiles throughout the day were not recorded on those days. When comparing the mean loads to the ice material properties in Table 1, it should be clarified that the material property tests were performed at the same time of day, at the end of the test day, on their respective days.

An examination of the specific time series of the low-speed tests where the velocity effect is observed (< 3 mm s^{-1}), and in particular at the start of those experiments, it was found that the higher loads were

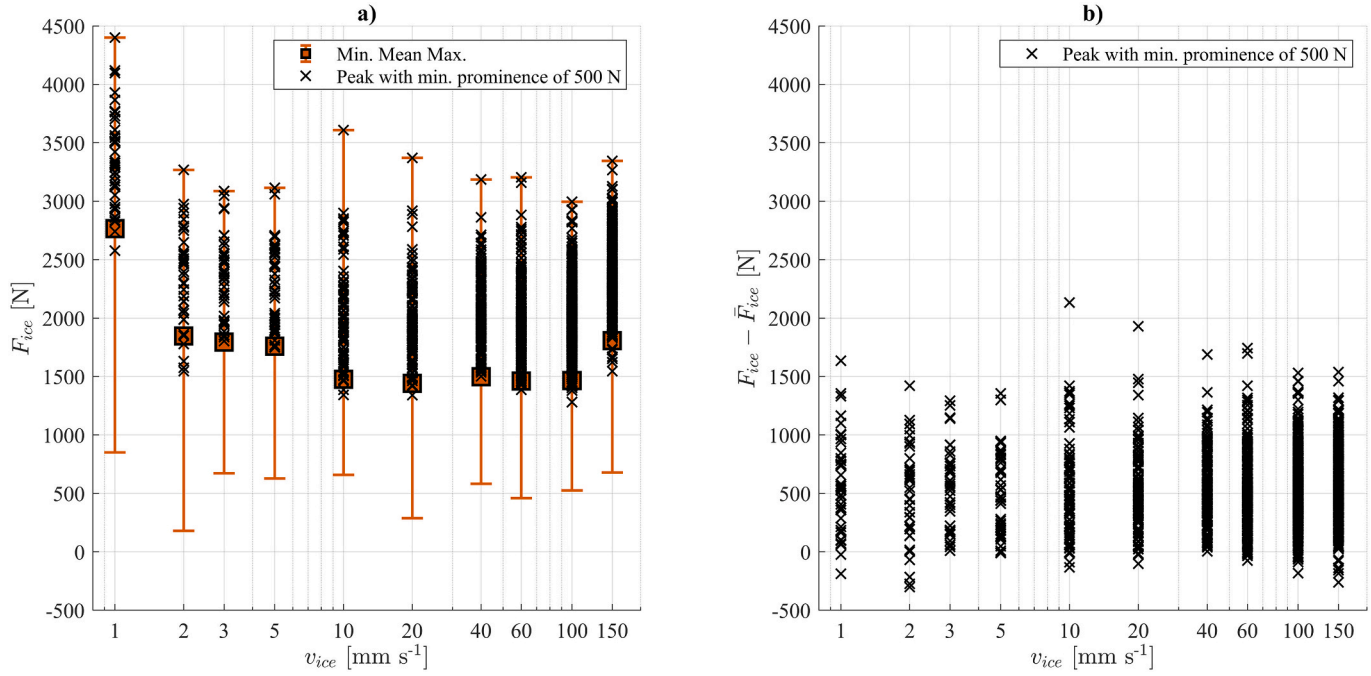

Fig. 4. a): Load-velocity dependence as obtained from rigid structure tests on the 17th of June. b): Mean load $\bar{F}_{ice}$ per test subtracted from the peaks. Peaks (black crosses) are selected based on a minimum peak prominence of 500 N. The minimum peak prominence is defined as the minimum relative height difference between peaks and determined by the *findpeaks* function in MATLAB.

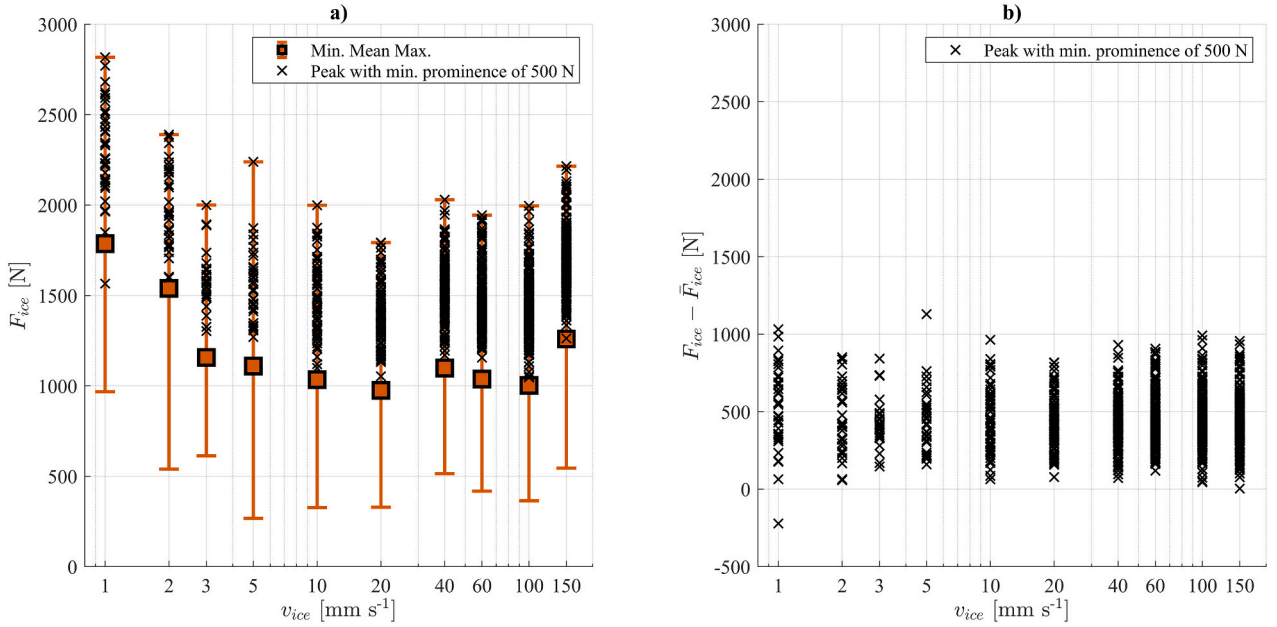

Fig. 5. a): Load-velocity dependence as obtained from rigid structure tests on the 23rd of June. b): Mean load $\bar{F}_{ice}$ per test subtracted from the peaks. Peaks (black crosses) are selected based on a minimum peak prominence of 500 N. The minimum peak prominence is defined as the minimum relative height difference between peaks and determined by the *findpeaks* function in MATLAB.

established within seconds. The first high peak load was attained within 1.3 s at 2 mm s^{-1} and within 3.2 s at 1 mm s^{-1} on the 23rd of June (see Fig. 6). On the 17th of June, for the same test conditions, the peak was achieved in about 2.4 s at 1 mm s^{-1}, though difficult to judge given a malfunction at the start of the test, and 1.8 s at 2 mm s^{-1}. Note that the high peak was not related to a full ice-structure contact upon initial loading as the test sequence was such that low-speed tests always followed a high-speed test. Also, the higher mean load established quickly and then remained constant as the test progressed. Although the exact test procedure is not reported here (see Hendrikse et al. (2022b) for more information), two important details are provided. First, the carriage or actuator (see Section 2.1) was stopped and the pile was moved away from the ice edge between changes in ice drift speed, with waiting intervals varying between roughly 5 s and 60 s. Second, because the pile was moved away from the ice edge, contact between the ice and pile was lost and zero load was measured between speed changes. Although ice strains were not measured in the experiments, these conditions likely had some effect on strain recovery in the ice sheet. By alternating between high- and low-speed tests in the procedure, an attempt was made to minimize damage and time-dependent strain related effects on the ice

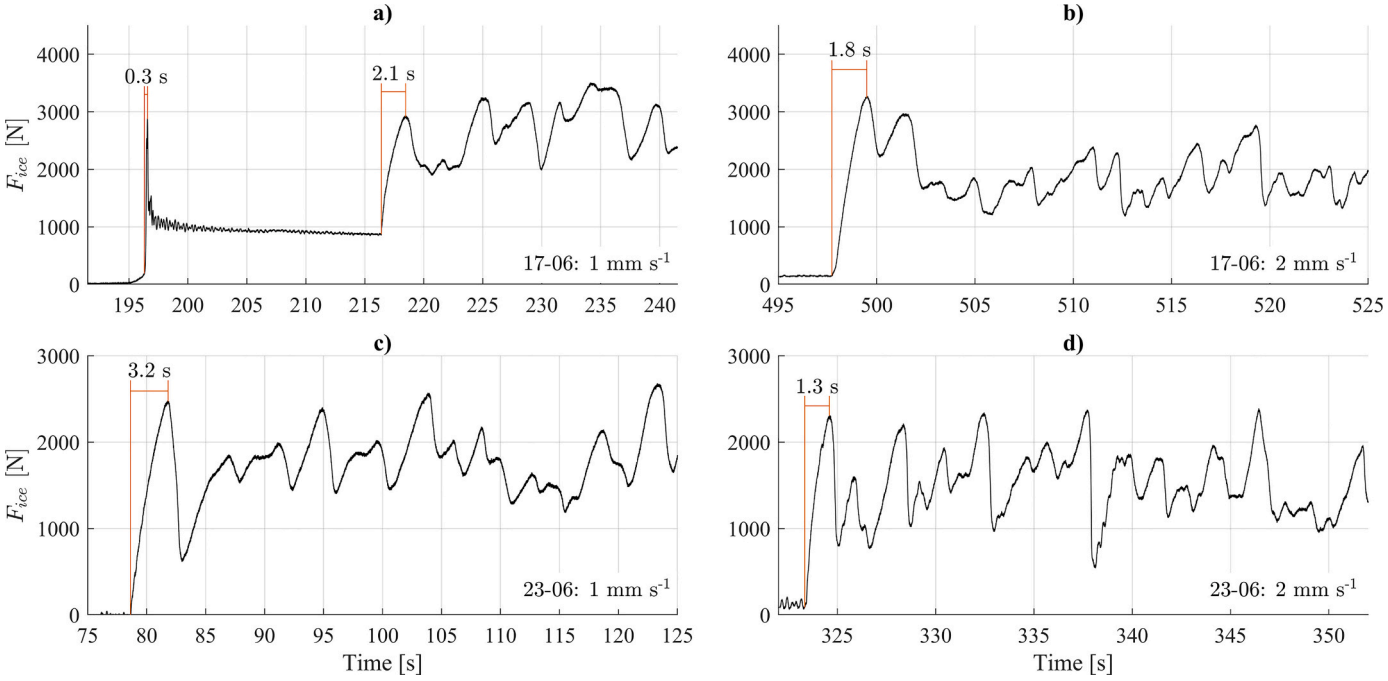

Fig. 6. Start of rigid structure ice penetration tests at low speed indicating the time to establish the first high peak load: a) at 1 mm s^{-1} on the 17th of June; b) at 2 mm s^{-1} on the 17th of June; c) at 1 mm s^{-1} on the 23rd of June; and d) at 2 mm s^{-1} on the 23rd of June.

load behavior from one test to another.

The consistent observation of higher mean and peak loads as a result of the loading history, specifically for low velocities in the case of the rigid structure tests, is henceforth referred to as an ice strengthening. The fact that this apparent strengthening of the ice manifested itself at the time scale of seconds is relevant for ice-structure interaction where the relevant time scales are governed by the natural periods of structures, often on the order of tenths of a second to several seconds. The compatibility between the time scales of ice strengthening and natural periods of structures indicates that a strengthening could develop during a cycle of interaction for such structures when the velocity of loading of the ice becomes sufficiently low. This compatibility in time scales in terms of rapid ice strengthening is relevant in assessing whether the mechanism causing the velocity effect on rigid structures is the same as that responsible for the compliance effect on flexible structures, which is further treated in Section 6. In the next section, the results from the controlled-oscillation tests are analyzed and compared to those in this section to investigate the dependence of the load-velocity relation on loading history.

4. The peak load-velocity dependence from controlled-oscillation tests

During the controlled-oscillation tests the relative velocity between ice and structure is not constant, but varies throughout the cycle of oscillation of the structure. This results in load peaks which occur within a range of relative velocities between ice and structure during each cycle of structural oscillation. Fig. 7 and Fig. 8 show the identified peak loads (using a minimum peak prominence of 500 N as determined by the *findpeaks* function in MATLAB) for the tests conducted on the 17th and 23rd of June, respectively. The arrows in Fig. 7 and Fig. 8 indicate if the relative velocity at the moment of failure was increasing (red color, rightward arrow) or decreasing (blue color, leftward arrow), defined as the sign of the derivative with respect to time of the relative velocity between ice and structure: $\text{signum}\left(\frac{d}{dt}[v_{ice}] - \frac{d^2}{dt^2}[Asin(\omega_c t)]\right)$. The peaks from the rigid structure tests in the same channel are included in the figures as well.

On both days, at high relative velocities ($>$ 20 mm s^{-1}), the peak loads found for the controlled-oscillation tests were in the same range as those observed for the rigid structure tests. This holds when the relative velocity is both increasing and decreasing (red and blue arrows, respectively). At lower velocities, in the range of 5 mm s^{-1} to 20 mm s^{-1}, a clear difference is found in the data from the 23rd of June (see Fig. 8). Peak loads for the controlled-oscillation tests are found to sometimes be higher than those for the rigid structure tests, but only when the loading rate was increasing (red arrows), with a few exceptions. However, the peak loads are not always higher when the relative velocity is increasing, as most red arrows reside in the range of peak loads observed for rigid structures (about 99% and 93% on the 17th and 23rd of June, respectively).

It seemed that the time spent, or duration, at a relative velocity in the lowest range, where a strengthening was also observed for the rigid structure, played a role in the higher peak loads. This is best illustrated when looking at both a time series of a test with many peaks exceeding those observed for a rigid structure and a time series of a test which follows the observations of a rigid structure as shown in Fig. 9. The tests both had an oscillation from 0 to 40 mm s^{-1} relative velocity, but the difference was in the frequency of oscillation. For the 4 Hz oscillation, the load pattern seemed to be mostly stochastic (see Fig. 9a). For the 0.5 Hz oscillation, however, the load pattern showed a clear periodicity (see Fig. 9b). Many cycles showed a high peak load after the moment when the zero relative velocity was reached. The main cause for the difference between the results seemed to be the amount of time spent at the low relative velocity. For the 0.5 Hz test, combined with a far-field constant ice drift speed of 20 mm s^{-1}, this was about 0.35 s below 3 mm s^{-1}. At 4 Hz and 20 mm s^{-1} constant far-field ice drift speed, this was about 0.04 s which appeared to be insufficient time to result in a significant increase in peak loads upon failure following the period of low relative velocity.

Referring again to Fig. 7, the results from the 17th of June did not appear to show this duration effect very strongly. This can be explained based on the test matrix of that day. Most controlled-oscillation tests were conducted at high far-field ice drift speeds and for high frequencies. In those cases, the time spent at low relative velocity was minimal.

For each test, the time spent at low relative velocity which can result in a strength increase can be estimated by means of a threshold velocity from the rigid structure experiments v_{thres} of 3 mm s^{-1}. The following equation then applies (Hendrikse and Metrikine, 2016):

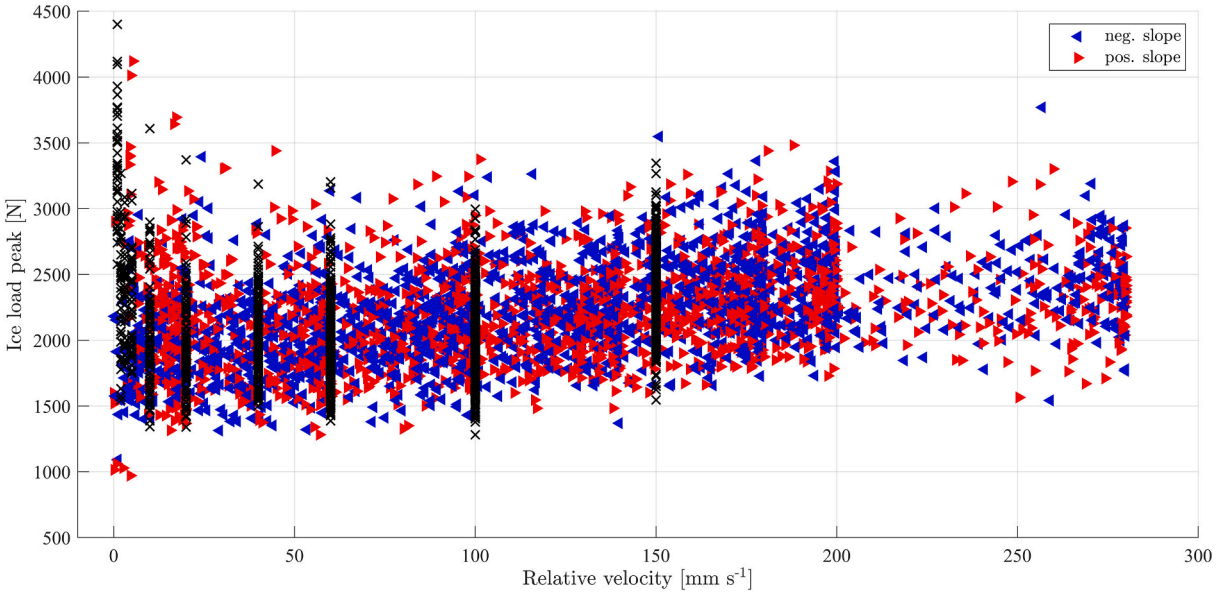

Fig. 7. Comparison of peak loads from controlled-oscillation tests (red and blue arrows, selected based on a minimum peak prominence of 500 N) and rigid structure tests (black crosses, see Fig. 4a) on the 17th of June. Arrows indicate the slope of relative velocity at the moment of failure: red, rightward arrows show positive slope; blue, leftward arrows show negative slope. (For interpretation of the references to colour in this figure legend, the reader is referred to the web version of this article.)

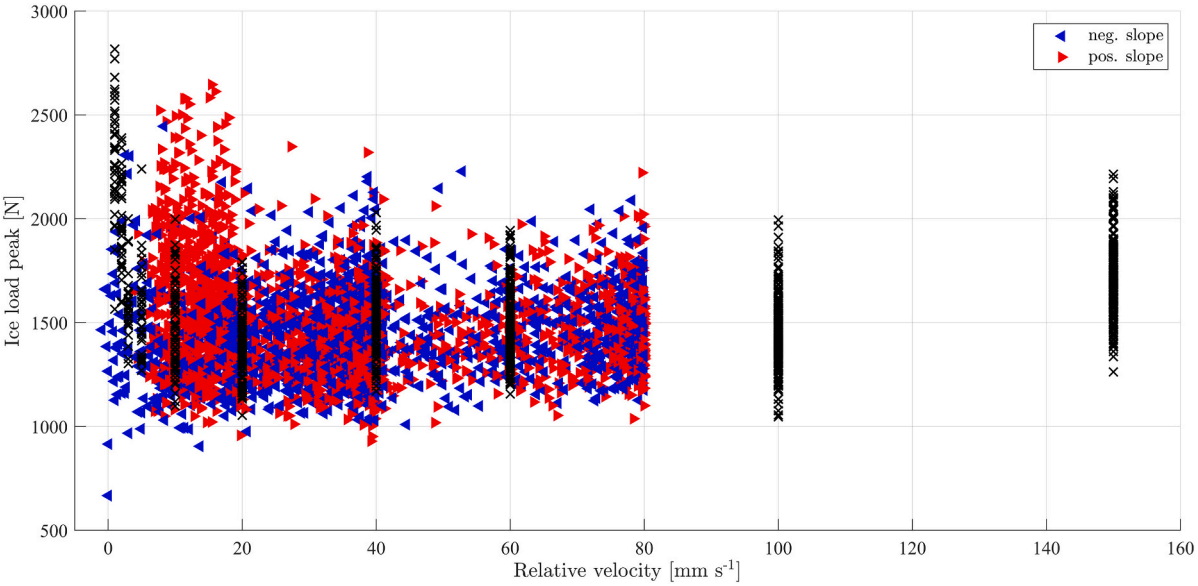

Fig. 8. Comparison of peak loads from controlled-oscillation tests (red and blue arrows, selected based on a minimum peak prominence of 500 N) and rigid structure tests (black crosses, see Fig. 5a) on the 23rd of June. Arrows indicate the slope of the relative velocity curve at the moment of failure of the ice: red, rightward arrows show positive slope; blue, leftward arrows show negative slope. (For interpretation of the references to colour in this figure legend, the reader is referred to the web version of this article.)

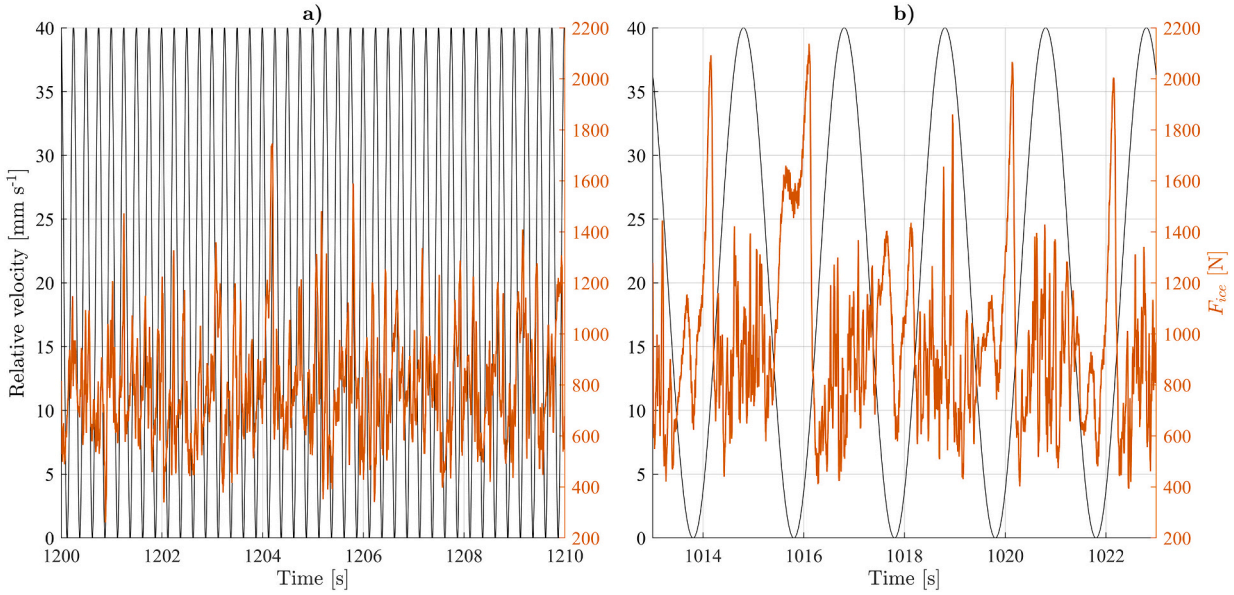

Fig. 9. Example results on the 23rd of June from a a) controlled-oscillation test (ID 504) showing peak loads in the same range as the rigid structure tests for the relative velocities included; and from b) controlled-oscillation test (ID 501) showing peak loads exceeding those on the rigid structure tests for the relative velocities included.

$$\Delta t = \frac{1}{(2\pi f)}\left(2arcsin\left(-1+\frac{v_{thres}}{v_{ice}}\right)+\pi\right) \tag{3}$$

In Fig. 10, the values of Δt for each of the controlled-oscillation tests are shown. On the 17th of June (left cluster in Fig. 10), two of the tests (ID 428 and 429) with the highest values of Δt are indicated and their times series are shown in Fig. 11. By inspecting each of the times series, the strengthening effect is indeed observed, though only significantly in test ID 428 (see Fig. 11a). For the controlled-oscillation tests with Δt below a threshold of about 0.3 s, the strengthening effect was no longer observed, which corresponds to the minimum time required for an observable strengthening effect from the rigid structure tests.

To summarize, a minimum duration seemed to be required at low relative velocity for mean and peak loads to surpass high-speed ice crushing loads, referred to as the ice strengthening effect, for the controlled-oscillation tests. For high ice drift speeds and high frequencies, the strengthening effect was not readily observed, which is consistent with the results of Eq. (3) in terms of little time spent at near-zero relative velocity. The strengthening in the controlled-oscillation tests resulted in the observation of peak loads which exceeded those for a rigid structure at the same far-field ice drift speeds. This matches with the definition of the compliance effect as shown in Fig. 1. In terms of far-field ice drift speeds, it is hence found that the peak load-velocity relation is load-history dependent and cannot be uniquely defined for ice penetration scenarios where the relative velocity enters the low-rate

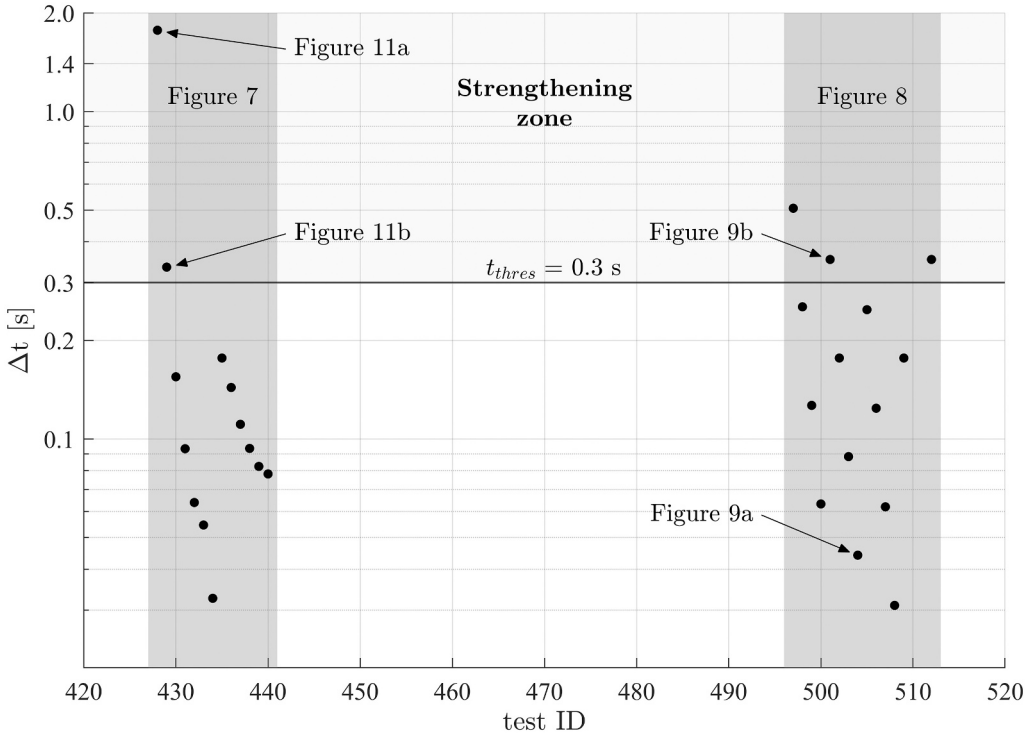

Fig. 10. The Δ*t* for each of the controlled-oscillation tests. The estimated minimum time t_{thres} required for an observable strengthening effect from the rigid structure tests is indicated by the horizontal line.

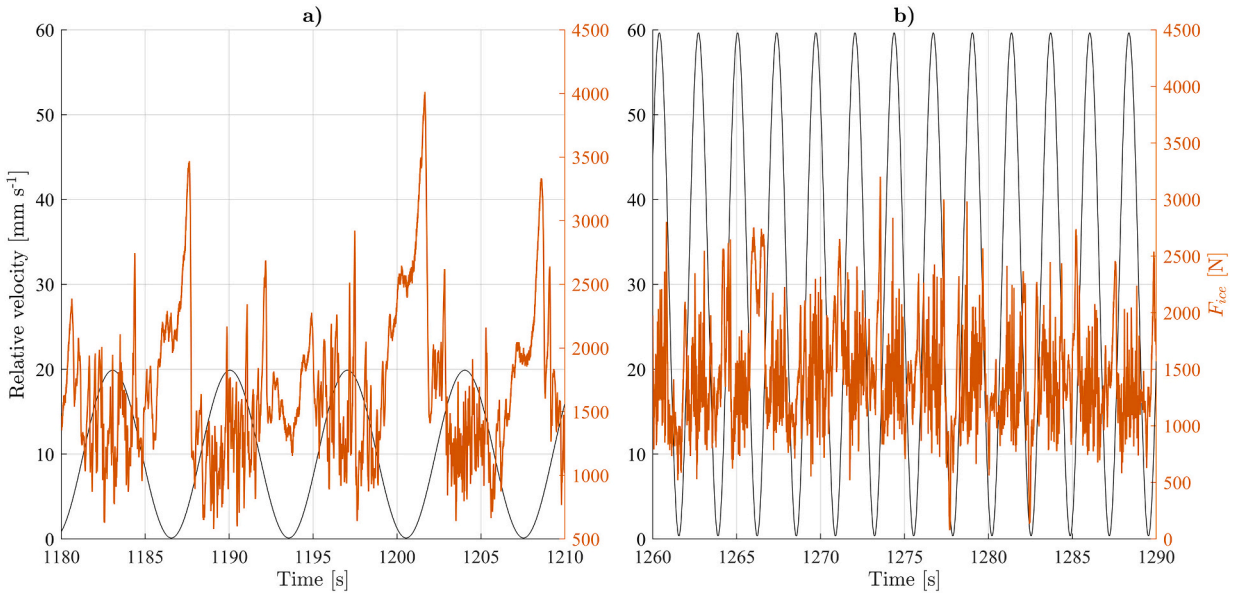

Fig. 11. Strengthening effect developing in the controlled-oscillation tests of a) test ID 428 on the 17th of June; and b) to a lesser extent in test ID 429 on the 17th of June.

regime for a sufficient duration to cause a strengthening of the ice.

The strengthening effect in the controlled-oscillation tests showed similarity to that observed for the rigid structure when considering the dependence on relative velocity instead of the far-field ice drift speed at the moment of the peak load. The reason for this is because the velocity experienced by the ice undergoing failure at the ice action point in the rigid structure tests is approximately equal to the far-field ice drift speed. Alternatively, in the controlled-oscillation tests, the velocity experienced by the ice undergoing failure is relative velocity. It thus follows that the velocity effect and compliance effect seem to originate from the same strengthening effect when relative velocity and not far-field ice drift speed is considered. To further substantiate this claim with respect to ice-induced vibrations, a SDOF structure test is analyzed in the next section, demonstrating that the strengthening effect indeed occurs during frequency lock-in and intermittent crushing.

5. The velocity and compliance effect during ice-induced vibrations

Fig. 12 shows results from a constant deceleration experiment with a

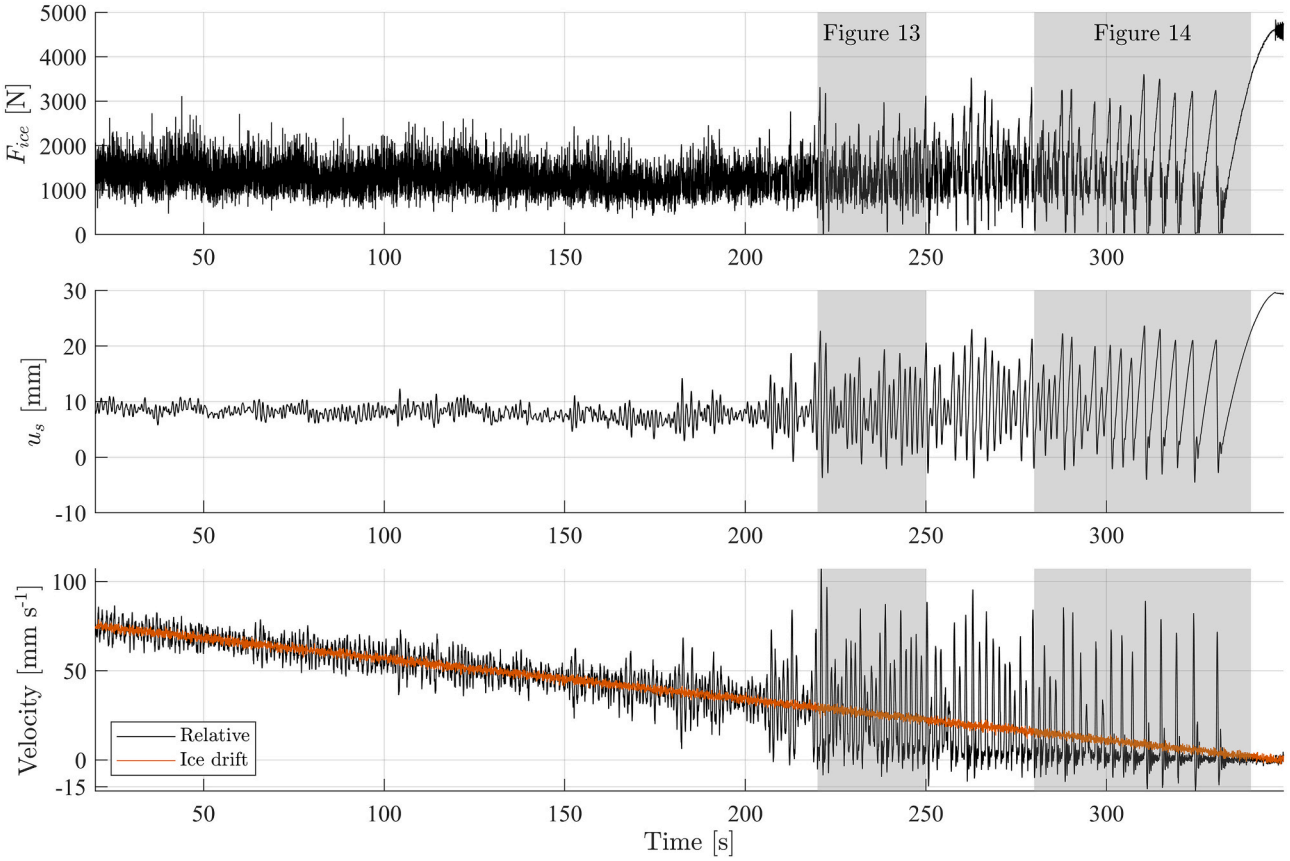

Fig. 12. Constant deceleration test (ID 445) with a single-degree-of-freedom structure on the 17th of June. Top: Ice load. Middle: Structural displacement. Bottom: Relative velocity and ice drift speed.

SDOF structure. This type of experiment was designed to resemble an ice floe slowing down and arresting against a flexible structure which in full-scale has been observed to result in frequency lock-in and intermittent crushing (Jefferies et al., 2008; Peyton, 1968). At high far-field ice drift speeds the relative velocity remains high and continuous brittle crushing is observed.

Frequency lock-in developed for the far-field speed range between 25 and 30 mm s^{-1} approximately, though only for a few consecutive cycles at a time (see Fig. 13). This type of interaction was accompanied by a duration of low, or even negative relative velocity. The strengthening effect clearly developed during the cycles of oscillation of the structure where high load peaks were observed after some duration of low relative velocity on the order of tenths of a second. Long sustained periods of frequency lock-in were typically only observed in tests with nearly constant far-field ice drift speed (van den Berg et al., 2022) as overly rapid constant deceleration tests resulted in a very brief transition from continuous brittle crushing to intermittent crushing.

For lower ice drift speeds ($<$ 15 mm s^{-1}), intermittent crushing clearly developed (see Fig. 14). Here, the relative velocity remained low until failure during the load build-up phase and the strengthening effect developed similarly to that of the rigid structure tests under constant far-field ice drift speed. In this comparison, the far-field ice drift speed of the rigid structure test was equal to the relative velocity of the SDOF structure test. Upon global failure and unloading, the relative velocity increased rapidly, typically by orders of magnitude, and the strengthening dissipated. At high relative velocity, multiple failures via brittle crushing ensued with peak loads much lower than those during the end of the load build-up phase. At the end of the test, the ice drift speed approached zero slowly and the ice load increased to $>$4 kN which is in accordance with that observed for the lowest speed tested for the rigid structure in Fig. 4.

Fig. 15a shows the peak loads from the SDOF structure test as a function of relative velocity as plotted in the same way as the controlled-oscillation test results in the previous section. It can be seen that the SDOF structure results show a similar load-history effect in peak loads as those from the controlled-oscillation tests. Higher peaks are observed for relative velocities in the range up to 10 mm s^{-1} when compared to a constant far-field ice drift speed for a rigid structure test. These peaks only develop after a period of loading of the ice at near-zero relative velocity and are associated with the events of frequency lock-in and intermittent crushing as shown in Fig. 13 and Fig. 14, respectively.

Fig. 15b shows the SDOF structure test results plotted, not for the relative velocity at the moment of peak load, but rather for the constant far-field ice drift speed. The comparison between Fig. 15a and Fig. 15b demonstrates how the effect of structural compliance could be misassociated with too high velocities when using this more common way of plotting peak loads against velocity as illustrated, for example, in Fig. 1. It should be noted that the peak loads exceeding those of the rigid structure tests (remaining red arrows) in Fig. 15 that do not correspond to the cases of frequency lock-in and intermittent crushing instead correspond to the peak loads before or between the two selected time series in Fig. 12 (between 20 s and 220 s, and between 250 s and 280 s).

6. Discussion

6.1. The peak load-velocity dependence during penetration and ice-induced vibrations

The foregoing observations and analysis indicate that the peak load-velocity dependence during ice penetration was found to be loading-history dependent. In cases where the relative velocity was constant, e.g. for rigid structures, the peak load-velocity dependence appeared to

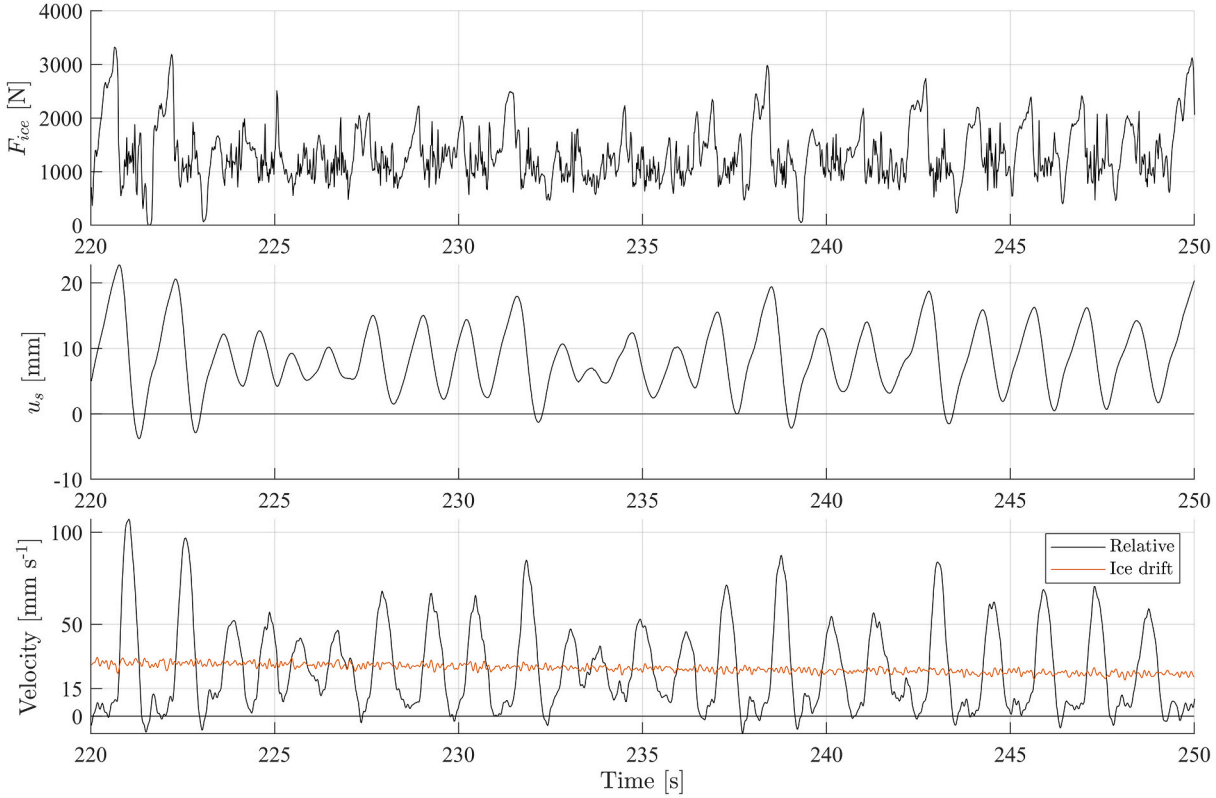

Fig. 13. Detailed view of frequency lock-in type oscillation occurring in test ID 445 (single-degree-of-freedom structure test). Top: Ice load. Middle: Structural displacement. Bottom: Relative velocity and ice drift speed.

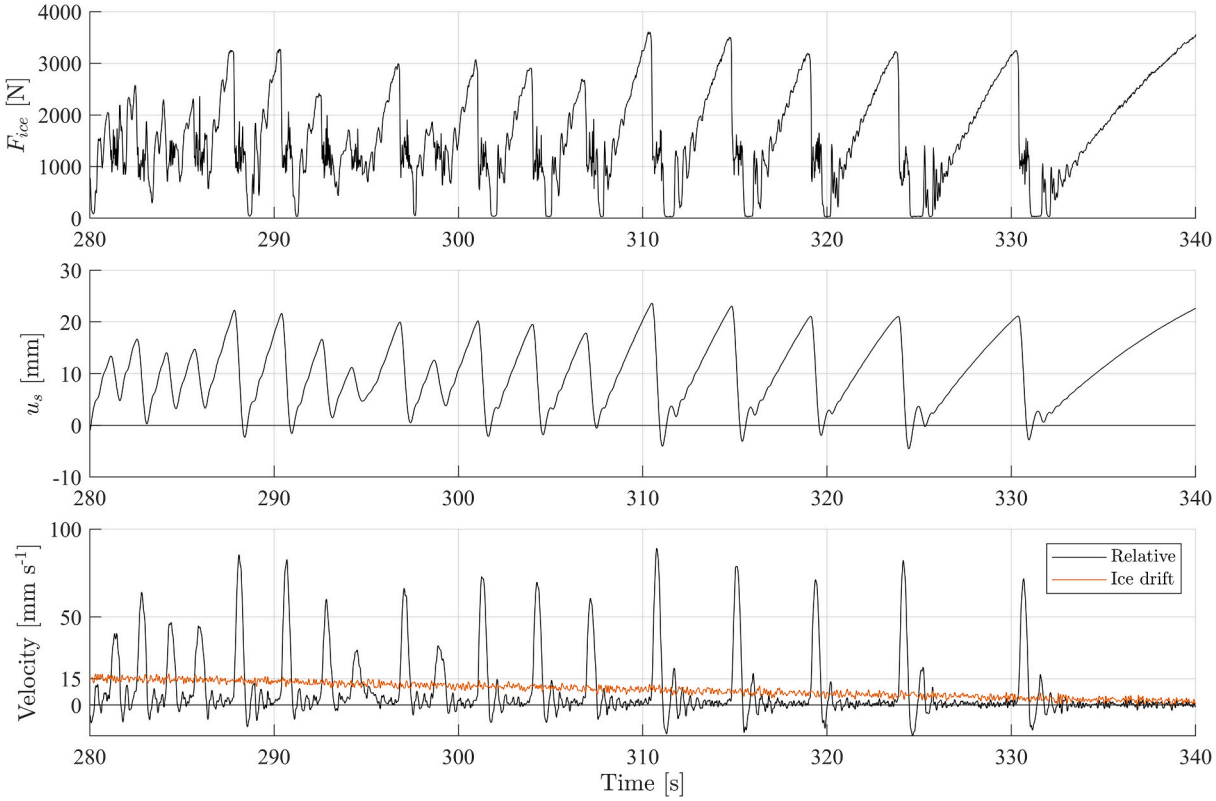

Fig. 14. Detailed view of intermittent crushing vibrations occurring in test ID 445 (single-degree-of-freedom structure test). Top: Ice load. Middle: Structural displacement. Bottom: Relative velocity and ice drift speed.

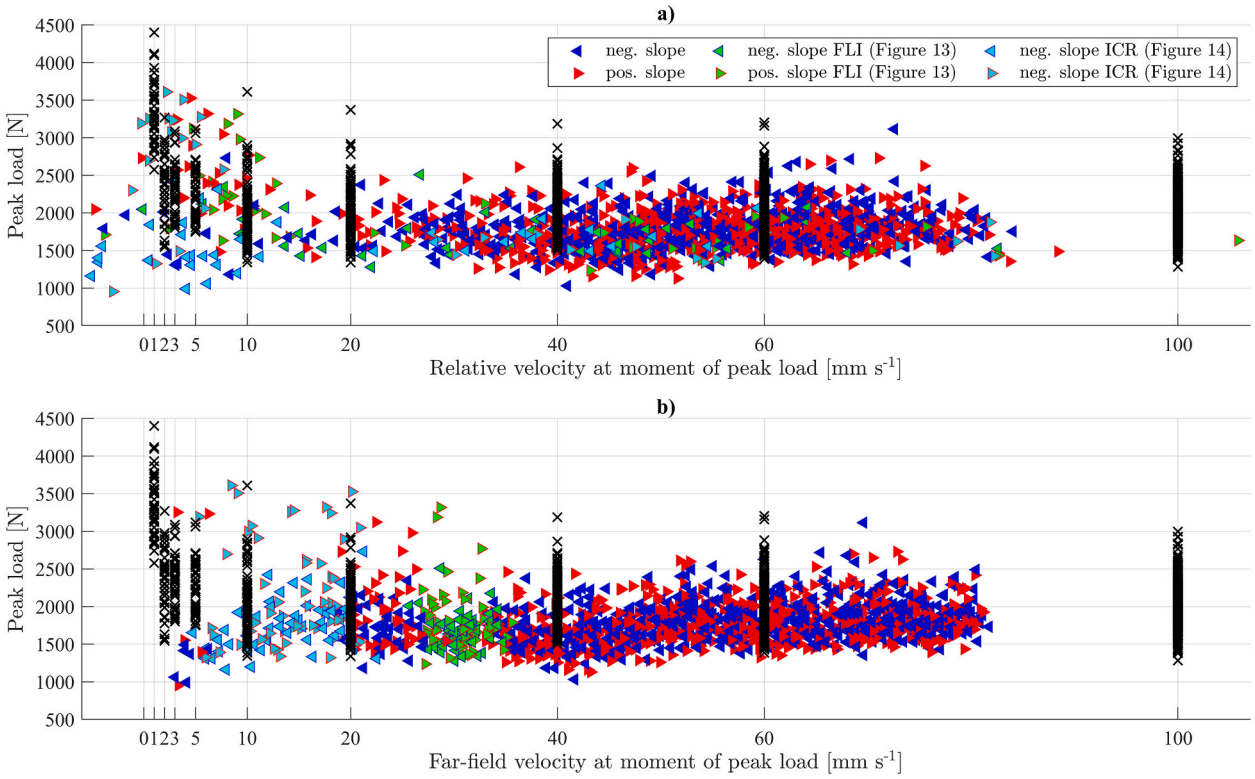

Fig. 15. Velocity and compliance effect example: a) peak loads from test ID 445 identified with a minimum peak prominence of 500 N, as a function of relative velocity at the moment of peak load; b) peak loads from test ID 445 (17th of June) identified with a minimum peak prominence of 500 N, as a function of far-field velocity at the moment of peak load. Peak loads from the rigid structure tests on 17th of June are marked by black crosses (see Fig. 4a). Arrows indicate the slope of relative velocity at the moment of failure: red, rightward arrows show positive slope; blue, leftward arrows show negative slope. The cases of frequency lock-in (FLI) and intermittent crushing (ICR) are identified by the green and cyan colors, respectively. (For interpretation of the references to colour in this figure legend, the reader is referred to the web version of this article.)

be uniquely defined. A velocity effect was observed as a rapid strengthening, within seconds, at low relative velocities. For cases where the relative velocity varied, but the time spent at low relative velocity was too short to activate the strengthening effect, the dependence remained uniquely defined; i.e. at the same far-field ice drift speed, the peak loads from the controlled-oscillation tests with high frequency and/or high ice drift speed did not exceed the peak loads from the rigid structure tests. However, when the time spent at low relative velocity was sufficient to activate the strengthening, the peak load-velocity relation showed a strong path dependence (see Fig. 8 and Fig. 15).

The strain and strain rate in the ice sheet were not measured in the experiments. Therefore, the dependence of the peak load-relative velocity relation on the stress-strain-rate relation could not be investigated. Nevertheless, a comment can be made about this dependence. Based on the analysis, it seemed that relative velocity and strain rate did not follow a linear relation because peak loads from controlled-oscillation tests were occasionally higher than those from the rigid structure tests. The particular path dependence of the peak loads from the controlled-oscillation tests may be related to damage, strain rate effects in the ductile-to-brittle transition in relatively undamaged ice, or a combination of both.

As there is a minimum amount of time associated with the strengthening effect, there should be a limit in terms of the maximum frequency for which frequency lock-in vibrations can develop. International Standard Organization (2019) refers to field observations of frequency lock-in up to 10 Hz. It would be of interest to determine the time constant associated with the strengthening process for different types of ice at different temperatures. This may allow the definition of a dimensionless number for ice-induced vibrations relating the time at low relative velocity during interaction to a characteristic time as a material property of the ice. This is left for further study.

In terms of modeling of ice-induced vibrations, it is important to note that models adopting a bijective relation between peak load and velocity do not correctly account for the loading history. The implied instantaneous strengthening of the ice occurs in those models (Kärnä, 1992; Määttänen, 1998; Withalm and Hoffmann, 2010) in cases where there is actually not sufficient time for the strengthening to develop. Models where the peak load-velocity relation develops as a result of a time-dependent strengthening effect can account for the load-history dependence (Hendrikse and Nord, 2019).

6.2. Compliance and velocity effects in ice peak loads

The results from the penetration experiments performed with the rigid structure, controlled oscillation, and SDOF structure in the present study show that peak loads depend on the amount of time spent at low relative velocities where a strengthening of the ice can develop. Both the velocity and compliance effects describe the scenario in which peak ice loads increase with low relative velocity. The observed compliance effect (see Fig. 15) likely originates from the same mechanism as the velocity effect seen for rigid structures as demonstrated with the controlled-oscillation tests. As stated previously, for ice acting with any velocity against a rigid structure, the far-field ice drift speed is equal to the relative velocity. For a compliant structure, the structural velocity needs to be subtracted from the far-field ice drift speed to result in a relative velocity, which shifts the strengthening effect to lower velocities as highlighted in Fig. 15. This shift is important with respect to design ice loads. If the effects indeed originate from the same mechanism, then the peak loads on a compliant structure cannot exceed those at the lowest speeds on a rigid structure. Indeed, International Standard

Organization (2019) states that the maximum loads on a compliant structure during intermittent crushing can be considered equal to the maximum loads on a rigid structure (Kärnä and Masterson, 2011). Based on our test results, this is a correct approach provided that the value used for C_R accounts for the velocity effect. It is further important to correctly interpret peak loads plotted against the far-field ice drift speed when the compliance effect is investigated since such plots can show peak loads at higher velocities than the actual relative velocity at the moment of failure (see Fig. 15).

6.3. Rapid strengthening at low relative velocity as a property of ice or model ice only

The observed rapid strengthening effect could be a property of model ice only. But since there is little evidence of tests on naturally occurring ice where the relative velocity was varied during penetration in a way as was done during the controlled-oscillation tests, this claim is difficult to confirm. Recent tests on the flexural strength of ice did, however, show a strengthening under cyclic loading which demonstrates that ice can exhibit such type of behavior (Murdza et al., 2021; Murdza et al., 2020). Similarly, cyclic biaxial compression of freshwater ice demonstrated strengthening by a factor of 1.5 in failure strength when subjected to moderate confinement and progressively higher loads (Iliescu and Schulson, 2002) Besides cyclic ice behavior, so-called damage or pre-straining in ice has shown to shift the ductile-to-brittle transition in ice to higher strain rates, thereby delaying failure in uniaxial compression experiments on both saline and freshwater ice (Snyder et al., 2016). A physical explanation for ice strengthening may be in the form of dislocation pile-ups or back stress development which relaxes over time and is enhanced by damage. A recent discussion on dislocation behavior in ice by Cole (2021) also showed there may be an explanation found in the low-speed deformation behavior and delayed elasticity of ice. In the past, the authors ascribed the strengthening to result from a change in the contact between ice and structure. A phenomenological model based on this idea has shown to be quite capable of simulating ice-induced vibrations (Hendrikse and Metrikine, 2015). Though the contact area change may be an artifact of the way measurements were made in the past with tactile sensors, as speculated by other researchers, the strengthening effect is real. Furthermore, even if the strengthening effect is related to a different physical mechanism in the ice, one could model it with the same phenomenological approach. Now that it is clearer where to investigate, it may be possible to develop a physics-based model which captures the strengthening, something which will allow for much more accurate prediction of full-scale dynamic ice-structure interaction.

6.4. Comment on spalling as a mechanism for ice-induced vibrations

In the experiments from the present study, ice-induced vibrations were found to develop as a result of strengthening of the ice when loaded for some tenths of a second at low relative velocities. An alternative mechanism for ice-induced vibrations has been proposed in the literature, which is the synchronization between the frequency associated with spalling of the ice and a natural frequency of the structure (Gagnon, 2022). In the experiments from the present study, it is found that multiple events of failure of the ice occur during each cycle of interaction, rather than just a single spalling event. During intermittent crushing, one of the failure events is related to the long load build-up phase with low relative velocity, but it is followed by multiple failure events during the unloading phase when the relative velocity is high (see Fig. 14). It could be speculated that the full-scale data from the Molikpaq do not show sufficient detail to discern the unloading phase (Owen and Hendrikse, 2021), leading to a misinterpretation that there is only a single failure event per saw-tooth cycle. Though it cannot be excluded based on the experiments in the present study that the spalling mechanism governs ice-induced vibrations in full-scale, it would, in the view of the authors, be a most interesting coincidence if model ice contains a completely different mechanism from sea ice which results in exactly the same complex ice-structure interaction phenomena.

7. Conclusion

The ice penetration experiments in model ice were performed with a rigid structure, controlled oscillation, and a SDOF structure, and comparison of results showed that the peak global ice loads depended on the amount of time spent at low relative velocities where an ice strengthening effect developed. Although the experiments were performed in ethanol-doped model ice of nominally 30 mm thickness with a pile of 200 mm in diameter, the consistency of the results and their similarity with the literature give support to the claim that the ice strengthening effect may be a general property of ice. This has implications for the so-called velocity effect and compliance effect in design of structures subject to dynamic ice-structure interaction. The main conclusions are summarized as follows:

1. The peak load-velocity dependence for ice penetration was not always uniquely defined as the loading history influenced the peak load prior to failure under the conditions of sufficient time spent at near-zero relative velocity.
2. Rapid ice strengthening developed at low relative velocities, which was carried over to high relative velocities until ice failure dissipated the strengthening effect.
3. The rapid ice strengthening resulted in peak loads, under the conditions of a varying relative velocity, which exceeded those for a constant penetration velocity, but only when the relative velocity increased from low to high values.
4. The ice strengthening effect was observed during each cycle of ice-induced vibrations in the present study, specifically for frequency lock-in and intermittent crushing, thereby causing the high peak loads observed during such interaction.
5. The velocity effect and compliance effect during penetration seemed to originate from the same strengthening effect, implying that absolute peak loads on compliant structures would not exceed those for the lowest speeds on rigid structures.
6. It is cautioned that assigning peak loads to the far-field ice drift speed for compliant structures may result in the attribution of high peak loads to velocities exceeding the actual relative velocities at which the peak loads develop.

Funding

This work was supported by TKI-Energy by the 'Toeslag voor Topconsortia voor Kennis en Innovatie (TKI's)' of the Dutch Ministry of Economic Affairs and Climate Policy. (grant reference: TKITOE_WOZ_1906_TUD_SHIVER).

CRediT authorship contribution statement

Cody C. Owen: Formal analysis, Investigation, Data curation, Writing – original draft. **Tim C. Hammer:** Investigation, Writing – review & editing, Visualization. **Hayo Hendrikse:** Conceptualization, Formal analysis, Investigation, Data curation, Writing – original draft, Supervision, Project administration, Funding acquisition.

Declaration of Competing Interest

The authors declare that they have no known competing financial interests or personal relationships that could have appeared to influence the work reported in this paper.

Data availability

The raw experimental data can be obtained from the

4TUResearchData repository (https://doi.org/10.4121/17087462.v1).

Acknowledgements

The authors thank the participating organizations in the SHIVER project: TU Delft and Siemens Gamesa Renewable Energy for supporting this work. The SHIVER project is co-financed by Siemens Gamesa Renewable Energy and TKI-Energy by the 'Toeslag voor Topconsortia voor Kennis en Innovatie (TKI's)' of the Dutch Ministry of Economic Affairs and Climate Policy. We further thank Jeroen Koning, Kees van Beek, and the colleagues from DEMO at TU Delft for the design and manufacturing of the mechanical parts of the test setup. We thank the crew of the Aalto Ice Tank: Teemu Päivärinta, Lasse Turja, and Sampo Hanhirova, for their help in preparation and installation of the setup and execution of the tests. And we are grateful to our colleagues Marnix van den Berg, Tom Willems, and Nick Ebben for the summer days in the cold executing the experiments.

Appendix A. Experimental data from test campaign

Experimental data for the present study have been selected from Hendrikse et al. (2022b) and are listed in Table A.2, Table A.3, and Table A.4 below.

Table A.2
Overview of rigid structure tests considered in the present study.

ID	Run name	Speed [mm s^{-1}]	Duration [s]	Time of day [HH:MM]
487	2306_1	100	19	09:28
488	2306_1	1	193	09:28
489	2306_1	40	21	09:32
490	2306_1	2	99	09:33
491	2306_1	150	11	09:34
492	2306_1	5	40	09:35
493	2306_1	60	21	09:36
494	2306_1	3	67	09:36
495	2306_1	20	31	09:38
496	2306_1	10	40	09:38
418	1706_10	100	21	16:09
419	1706_10	1	197	16:10
420	1706_10	40	21	16:14
421	1706_10	2	100	16:15
422	1706_10	150	10	16:17
423	1706_10	5	41	16:18
424	1706_10	60	21	16:19
425	1706_10	3	67	16:20
426	1706_10	20	31	16:22
427	1706_10	10	42	16:23

Table A.3
Overview of controlled-oscillation tests considered in the present study.

ID	Run name	v_{ice} [mm s^{-1}]	f_c [Hz]	A [mm]	Time of day [HH:MM]
428	1706_10	10	0.143	11.00	16:25
429	1706_10	30	0.429	11.00	16:27
430	1706_10	50	0.716	11.00	16:29
431	1706_10	70	1.002	11.00	16:30
432	1706_10	90	1.289	11.00	16:30
433	1706_10	100	1.432	11.00	16:31
434	1706_10	140	2.025	11.00	16:32
435	1706_10	20	1.000	3.20	16:33
436	1706_10	30	1.000	4.80	16:34
437	1706_10	50	1.000	7.95	16:35
438	1706_10	70	1.000	11.10	16:36
439	1706_10	90	1.000	14.30	16:37
440	1706_10	100	1.000	15.90	16:37
497	2306_1	10	0.500	3.18	09:39
498	2306_1	10	1.000	1.59	09:40
499	2306_1	10	2.000	0.80	09:42
500	2306_1	10	4.000	0.40	09:43
501	2306_1	20	0.500	6.37	09:44
502	2306_1	20	1.000	3.18	09:45
503	2306_1	20	2.000	1.59	09:46
504	2306_1	20	4.000	0.80	09:47
505	2306_1	40	0.500	12.73	09:48
506	2306_1	40	1.000	6.37	09:49
507	2306_1	40	2.000	3.18	09:50
508	2306_1	40	4.000	1.59	09:51
509	2306_1	20	1.000	3.18	09:52
512	2306_1	20	0.500	6.37	09:55

Table A.4
Overview of single-degree-of-freedom structure tests considered in the present study.

ID	Run name	v_{ice} [mm s^{-1}]	f_s [Hz]	m_s [kg]	ζ_s [%]	Time of day [HH:MM]
445	1706_11	Ramp	0.889 Hz	5020	10.6	17:06

References

Cole, D.M., 2021. A constitutive model for sea ice: physical basis, formulations, examples and applications. In: Proceedings of the 26th International Conference on Port and Ocean Engineering under Arctic Conditions. POAC, Moscow, Russia, pp. 1–12.

Gagnon, R., 2022. Spallation-based numerical simulations of ice-induced vibration of structures. Cold Reg. Sci. Technol. 194, 103465 https://doi.org/10.1016/j.coldregions.2021.103465.

Hammer, T.C., van Beek, K., Koning, J., Hendrikse, H., 2021. A 2D test setup for scaled real-time hybrid tests of dynamic ice- structure interaction. In: Proceedings of the 26th International Conference on Port and Ocean Engineering under Arctic Conditions. POAC, Moscow, Russia, pp. 1–13.

Hammer, T.C., Owen, C.C., van den Berg, M., Hendrikse, H., 2022. Classification of Ice-Induced Vibration Regimes of Offshore Wind Turbines. In: Proceedings of the ASME 2022 41st International Conference on Ocean, Offshore and Arctic Engineering. American Society of Mechanical Engineers, Hamburg, Germany, pp. 1–8. https://doi.org/10.1115/OMAE2022-78972.

Hammer, T.C., Willems, T., Hendrikse, H., 2023. Dynamic ice loads for offshore wind support structure design. Mar. Struct. 87, 103335 https://doi.org/10.1016/j.marstruc.2022.103335.

Hendrikse, H., Metrikine, A., 2015. Interpretation and prediction of ice induced vibrations based on contact area variation. Int. J. Solids Struct. 75–76, 336–348. https://doi.org/10.1016/j.ijsolstr.2015.08.023.

Hendrikse, H., Metrikine, A., 2016. Edge indentation of ice with a displacement-controlled oscillating cylindrical structure. Cold Reg. Sci. Technol. 121, 100–107. https://doi.org/10.1016/j.coldregions.2015.10.013.

Hendrikse, H., Nord, T.S., 2019. Dynamic response of an offshore structure interacting with an ice floe failing in crushing. Mar. Struct. 65, 271–290. https://doi.org/10.1016/j.marstruc.2019.01.012.

Hendrikse, H., Hammer, T.C., Owen, C.C., van den Berg, M., van Beek, K., Polojärvi, A., Puolakka, O., Willems, T., 2022a. Ice Basin Tests for ice-induced vibrations of offshore structures in the SHIVER Project. In: Proceedings of the ASME 2022 41st International Conference on Ocean. Offshore and Arctic Engineering. American Society of Mechanical Engineers, Hamburg, Germany, pp. 1–9. https://doi.org/10.1115/OMAE2022-78507.

Hendrikse, H., Hammer, T.C., van den Berg, M., Willems, T., Owen, C.C., van Beek, K., Ebben, N.J.J., Puolakka, O., Polojärvi, A., 2022b. Experimental data from ice basin tests with vertically sided cylindrical structures. Data Br. 41, 107877 https://doi.org/10.1016/j.dib.2022.107877.

Hetmanczyk, S., Heinonen, J., Strobel, M., 2011. Dynamic ice load model in overall simulation of offshore wind turbines. In: Proceedings of the 21st International Offshore and Polar Engineering Conference. ISOPE, Maui, Hawaii, USA, pp. 347–352.

Huang, G., Liu, P., 2009. A dynamic model for ice-induced vibration of structures. J. Offshore Mech. Arct. Eng. 131, 1–6. https://doi.org/10.1115/1.2979795.

Iliescu, D., Schulson, E.M., 2002. Brittle compressive failure of ice: Monotonic versus cyclic loading. Acta Mater. 50, 2163–2172. https://doi.org/10.1016/S1359-6454(02)00060-5.

International Standard Organization, 2019. ISO 19906 Petroleum and Natural gas Industries - Arctic Offshore Structures.

ITTC, 2014. Test Methods for Model Ice Properties. ITTC Quality System Manual, Recommended Procedures and Guidelines..

Izumiyama, K., Irani, M.B., Timco, G.W., 1994. Influence of compliance of structure on ice load. In: Proceedings of the 12th IAHR International Symposium on Ice. IAHR, Trondheim, Norway, pp. 229–238.

Jefferies, M., Kärnä, T., Løset, S., 2008. Field data on the magnification of ice loads on vertical structures. In: Jasek, M. (Ed.), Proceedings of the 19th IAHR International Symposium on Ice. IAHR, Vancouver, British Columbia, Canada, pp. 1325–1343.

Kamesaki, K., Yamauchi, Y., Kärnä, T., 1996. Ice force as a function of structural compliance. In: Proceedings of the 13th IAHR International Symposium on Ice. IAHR, Beijing, China, pp. 395–402.

Kärnä, T., 1992. a procedure for dynamic soil-structure-ice interaction. In: Proceedings of the 2nd International Offshore and Polar Engineering Conference. ISOPE, San Francisco, California, USA, pp. 764–771.

Kärnä, T., Masterson, D.M., 2011. Data for crushing formula. In: Proceedings of the 21st International Conference on Port and Ocean Engineering under Arctic Conditions. POAC, Montréal, Canada, pp. 1–12.

Kärnä, T., Guo, F., Løset, S., Määttänen, M., 2008. Small-scale data on magnification of ice loads on vertical structures. In: Jasek, M. (Ed.), Proceedings of the 19th IAHR International Symposium on Ice. IAHR, Vancouver, British Columbia, Canada, pp. 1313–1324.

Määttanen, M., 1981. Laboratory tests for dynamic ice-structure interaction. Eng. Struct. 3, 111–116. https://doi.org/10.1016/0141-0296(81)90037-7.

Määttänen, M.P., 1998. Numerical model for ice-induced vibration load lock-in and synchronization. In: Proceedings of the 14th IAHR International Symposium on Ice. IAHR, Potsdam, New York, USA, pp. 923–930.

Murdza, A., Schulson, E.M., Renshaw, C.E., 2020. Strengthening of columnar-grained freshwater ice through cyclic flexural loading. J. Glaciol. 66, 556–566. https://doi.org/10.1017/jog.2020.31.

Murdza, A., Schulson, E.M., Renshaw, C.E., 2021. Behavior of saline ice under cyclic flexural loading. Cryosph. 15, 2415–2428. https://doi.org/10.5194/tc-15-2415-2021.

Owen, C.C., Hendrikse, H., 2021. Simulation and analysis of ice-induced vibrations experienced by Molikpaq during the May 12, 1986 event. In: Proc 26th Int. Conf. Port Ocean Eng. Under Arct. Cond. POAC 2021-June, pp. 1–14.

Peyton, H.R., 1968. Sea ice forces. Proceed. Conf. Ice Pressur. Against Struct. 117–123.

Singh, S.K., Timco, G.W., Frederking, R.M.W., Jordaan, I.J., 1990. Tests of ice crushing on a flexible structure. In: Proceedings of the 9th Offshore Mechanics and Arctic Engineering Symposium. OMAE, Houston, Texas, USA, pp. 89–94.

Snyder, S.A., Schulson, E.M., Renshaw, C.E., 2016. Effects of prestrain on the ductile-to-brittle transition of ice. Acta Mater. 108, 110–127. https://doi.org/10.1016/j.actamat.2016.01.062.

Sodhi, D.S., 2001. Crushing failure during ice-structure interaction. Eng. Fract. Mech. 68, 1889–1921. https://doi.org/10.1016/S0013-7944(01)00038-8.

Tsuchiya, M., Kanie, S., Ikejiri, K., Yoshida, A., Saeki, H., 1985. An experimental study on ice-structure interaction. In: Proceedings of the 7th Offshore Technology Conference. Offshore Technology Conference, Houston, Texas, USA, pp. 312–327. https://doi.org/10.4043/5055-MS.

van den Berg, M., Owen, C.C., Hendrikse, H., 2022. Experimental study on ice-structure interaction phenomena of vertically sided structures. Cold Reg. Sci. Technol. 201, 103628 https://doi.org/10.1016/j.coldregions.2022.103628.

Withalm, M., Hoffmann, N.P., 2010. Simulation of full-scale ice-structure-interaction by an extended Matlock-model. Cold Reg. Sci. Technol. 60, 130–136. https://doi.org/10.1016/j.coldregions.2009.09.006.